ELSEVIER

International Journal of Solids and Structures 41 (2004) 2259–2276

INTERNATIONAL JOURNAL OF SOLIDS and STRUCTURES

www.elsevier.com/locate/ijsolstr

A comparison between a 3D discrete model and two homogenised plate models for periodic elastic brickwork

Antonella Cecchi [a,*], Karam Sab [b,1]

[a] *Dipartimento di Costruzione dell'Architettura D.C.A., Università degli Studi I.U.A.V., ex convento Terese, Dorsoduro Venezia 2206, 30123 Italy*

[b] *LAMI (ENPC-LCPC, Institut Navier) 6 and 8 avenue Blaise Pascal, Cité Descartes F-77455, Marne-La-Vallée Cedex 2, France*

Received 10 December 2003; received in revised form 10 December 2003

Abstract

A Love–Kirchhoff plate model for in plane and out of plane actions of linear elastic periodic brickwork has been already proposed by Cecchi and Sab [Eur. J. Mech. A.-Solids, 21 (2002a) 249]. In this work, the case of infinitely rigid blocks connected by elastic interfaces (the mortar thin joints) is considered. A numerical discrete 3D model is proposed and compared to the homogenised Love–Kirchhoff plate model. In order to enhance this plate model, shear effects are taken into account leading to the identification of a new Reissner–Mindlin homogenised plate model. The bending constants of both Love–Kirchhoff and Reissner–Mindlin models are the same, while the shear constants of the Reissner–Mindlin model are identified using a simple procedure of compatible identification between the 3D discrete model and the 2D one. A numerical evaluation of the scatter between the 3D discrete model and both Love–Kirchhoff and Reissner–Mindlin models is performed on a test case for various values of the ratio between the thickness of the wall and its overall size, and for various values of the parameter that characterises the heterogeneity of the wall. It is shown that both plate models coincide asymptotically with the discrete 3D model, the convergence being better for the Reissner–Mindlin model.

Keywords: Heterogeneous; Periodic structure; Elasticity; Masonry; Kirchhoff plates; Mindlin plates; Discrete models

1. Introduction

Masonry is a heterogeneous material obtained by the regular repetition of blocks between which mortar is laid. By periodic brickwork the reference was set to a masonry made either by dry stone blocks or by brick blocks connected through thin mortar joints and arranged according to a periodic texture. An extensive literature has been developed to obtain a description of discrete systems by means of

* Corresponding author. Tel.: +39-041-2571288; fax: +39-041-5223627.
E-mail addresses: cecchi@brezza.iuav.it (A. Cecchi), sab@lami.enpc.fr (K. Sab).
[1] Tel.: +33-1-64153749.

0020-7683/$ - see front matter © 2004 Elsevier Ltd. All rights reserved.
doi:10.1016/j.ijsolstr.2003.12.020

microstructural approach (Alpa and Monetto, 1994; Anthoine and Pegon, 1994; Anthoine, 1995; Lee et al., 1996, 1998; Luciano and Sacco, 1997; Masiani et al., 1995; Lopez et al., 1999).

By reference to the continuum models, 2D rigorous homogenisation models in several perturbative parameters have been already developed—by Cecchi and Rizzi (2001) and Cecchi and Sab (2002a)—in order to study the behaviour of masonry walls subject to actions parallel to the middle plane. An asymptotic study in several parameters was also carried out by de Felice (1995) and an analytical solution was obtained for running bond. This model considered the case in which the blocks are rigid bodies and the thickness of mortar is zero. The mortar was modelled as an interface with a constitutive function that was directly assigned as a linear elastic function of the displacement jump across the joint. The solution of the auxiliary field problem on the representative unit cell was obtained analytically because of the rigid motions of the blocks. Then, the proposed expression for the homogenised stiffness tensor was only dependent on the geometry of the blocks and on the constitutive function of the interface.

Cecchi and Sab (2002b) developed also a plate model to study masonry walls subject to both in plane and out of plane actions through a rigorous homogenisation procedure. In this model, masonry is assumed periodic in the middle plane, i.e. in the orthogonal directions to its thickness. Another parameter, $\zeta \approx \varepsilon$, is added to the ε scale parameter typical of homogenisation methods. This new parameter is the ratio between the thickness t of the wall and its overall size L.

$$\varepsilon = \frac{a}{L} \ll 1 \quad \zeta = \frac{t}{L} \ll 1$$

where a is the in plane dimension of the representative unit cell (Sanchez-Palencia, 1980; Caillerie, 1984; Sanchez-Palencia and Zaoui, 1987; Sanchez-Hubert and Sanchez-Palencia, 1992).

If t is comparable to a, then the asymptotic model that has been developed allows the identification of the 3D heterogeneous solid with a 2D Love–Kirchhoff homogeneous plate in which the anisotropy is connected with the arrangement of blocks. Moreover, an analytical expression of the homogenised plate elastic constants was obtained when the blocks are rigid bodies. This hypothesis is representative of historical masonry; in fact, blocks are generally much stiffer than mortar and mortar joints show a very small thickness if compared with the sizes of the blocks.

The first purpose of this work is to evaluate the reliability of the previously mentioned Love–Kirchhoff homogenised model when compared to a discrete 3D model. Actually, similar comparison has been already developed by Salerno and de Felice (1999), Salerno and de Felice (2000) in the context of 2D homogenisation.

The second purpose is to enhance the Love–Kirchhoff model by taking into account the shear effects. Indeed, a Reissner–Mindlin model is identified—based on a compatible identification procedure—and a comparison with the 3D discrete model is carried out.

In Section 2 the discrete 3D model is presented; the blocks that form the masonry wall are modelled as rigid bodies connected by elastic interfaces (mortar thin joints). In other words, masonry is seen as a "molecular skeleton" in which the interactions between the molecules (rigid blocks) are represented by forces and moments which depend on their relative displacements and rotations (Lofti and Benson Shing, 1994; Lourenço and Rots, 1993; Markov, 1999).

In Section 3, the Reissner–Mindlin plate model is proposed and an identification of the shear elastic constants is performed.

In Section 4, the numerical results are shown. An evaluation of the scatter between the discrete model and the homogenised models is performed for various values of parameters ζ and ε. It is shown that both Love–Kirchhoff model and Reissner–Mindlin model coincide asymptotically with the discrete 3D model as $\zeta \approx \varepsilon$ tend to zero. Besides, the convergence is shown to be better for the Reissner–Mindlin model.

2. The 3D discrete model

Let $\mathbf{y}^{i,j}$ be the position of the centre of the generic $B_{i,j}$ block (Fig. 1) in the 3D Euclidean space:

$$\mathbf{y}^{i,j} = i\frac{b}{2}\mathbf{e}_1 + ja\mathbf{e}_2$$

where b is the width of the block and a is the height of the block. As shown by Fig. 1, j can actually take arbitrary values while i is such as $i+j$ is even. The displacement of each block is a rigid body motion:

$$\mathbf{u} = \mathbf{u}^{i,j} + \boldsymbol{\Omega}^{i,j} \wedge (\mathbf{y} - \mathbf{y}^{i,j}), \quad \forall \mathbf{y} \in B_{i,j} \tag{1}$$

where $\mathbf{u}^{i,j}$ is the translation vector and $\boldsymbol{\Omega}^{i,j}$ is the rotation vector of $B_{i,j}$.

Due to the regularity of the masonry structure, the $B_{i,j}$ block interacts with the $B_{i+k_1,j+k_2}$ block by means of Σ_{k_1,k_2} elastic joints as follows:

- if $k_1, k_2 = \pm 1$, then Σ_{k_1,k_2} is an horizontal interface;
- if $k_1 = \pm 2$ and $k_2 = 0$, then Σ_{k_1,k_2} is a vertical interface. The interfaces of the $B_{0,0}$ block are:

$$\Sigma_{-1,-1} = \begin{pmatrix} -\frac{b}{2} \leqslant y_1 \leqslant 0 \\ y_2 = -\frac{a}{2} \\ -\frac{t}{2} \leqslant y_3 \leqslant \frac{t}{2} \end{pmatrix}; \quad \Sigma_{+1,-1} = \begin{pmatrix} 0 \leqslant y_1 \leqslant \frac{b}{2} \\ y_2 = -\frac{a}{2} \\ -\frac{t}{2} \leqslant y_3 \leqslant \frac{t}{2} \end{pmatrix}$$

$$\Sigma_{+1,+1} = \begin{pmatrix} 0 \leqslant y_1 \leqslant \frac{b}{2} \\ y_2 = \frac{a}{2} \\ -\frac{t}{2} \leqslant y_3 \leqslant \frac{t}{2} \end{pmatrix}; \quad \Sigma_{-1,+1} = \begin{pmatrix} -\frac{b}{2} \leqslant y_1 \leqslant 0 \\ y_2 = \frac{a}{2} \\ -\frac{t}{2} \leqslant y_3 \leqslant \frac{t}{2} \end{pmatrix}$$

$$\Sigma_{+2,0} = \begin{pmatrix} y_1 = \frac{b}{2} \\ -\frac{a}{2} \leqslant y_2 \leqslant \frac{a}{2} \\ -\frac{t}{2} \leqslant y_3 \leqslant \frac{t}{2} \end{pmatrix}; \quad \Sigma_{-2,0} = \begin{pmatrix} y_1 = -\frac{b}{2} \\ -\frac{a}{2} \leqslant y_2 \leqslant \frac{a}{2} \\ -\frac{t}{2} \leqslant y_3 \leqslant \frac{t}{2} \end{pmatrix}$$

If the mortar joint is modelled as an elastic interface—such problem has been studied by Klarbring (1991) by means of perturbative techniques—, the deformation between two blocks may be written as a function of the displacement jump. The constitutive prescription for the contact is a linear relation between the tractions on the block surfaces and the jump of the displacement field.

$$\boldsymbol{\sigma}\mathbf{n} = \mathbf{K}[[\mathbf{u}]] \quad \text{on } \Sigma_{k_1,k_2} \tag{2}$$

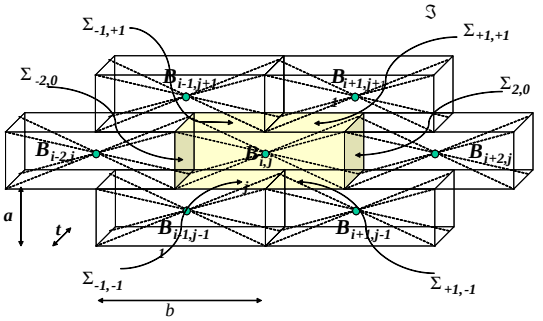

Fig. 1. Masonry structure.

Here $\boldsymbol{\sigma}$ is the stress tensor, $\mathbf{n}$ is the normal to Σ_{k_1,k_2}, $[[\mathbf{u}]]$ is the jump of the displacement field at Σ_{k_1,k_2} and $\mathbf{K}$ is given by

$$\mathbf{K}_{ij} = \frac{1}{e}\mathbf{a}^M_{iklj}\mathbf{n}_k\mathbf{n}_l \tag{3}$$

where $\mathbf{a}^M$ is the elastic stiffness tensor of the mortar and e is the thickness of the real joint. It will be assumed in the sequel that the mortar is isotropic, then Eq. (3) becomes:

$$\mathbf{K} = \frac{1}{e}\left(\mu^M\mathbf{I} + (\mu^M + \lambda^M)(\mathbf{n}\otimes\mathbf{n})\right) \tag{4}$$

where μ^M and λ^M are the Lamé constants of the mortar (Klarbring, 1991; Avila-Pozos et al., 1999; Cecchi and Sab, 2002a,b). Note that $\mathbf{K}$ tensor has a diagonal form in this case.

The interactions between the blocks through the interfaces are represented by elastic forces and moments that must be found. The following notations are introduced:

$$\Delta_1^{k_1,k_2} = u_1^{i+k_1,j+k_2} - u_1^{i,j} + k_2 a\frac{\Omega_3^{i+k_1,j+k_2} + \Omega_3^{i,j}}{2} \tag{5}$$

$$\Delta_2^{k_1,k_2} = u_2^{i+k_1,j+k_2} - u_2^{i,j} - k_1\frac{b}{2}\frac{\Omega_3^{i+k_1,j+k_2} + \Omega_3^{i,j}}{2} \tag{6}$$

$$\Delta_3^{k_1,k_2} = u_3^{i+k_1,j+k_2} - u_3^{i,j} + k_1\frac{b}{2}\frac{\Omega_2^{i+k_1,j+k_2} + \Omega_2^{i,j}}{2} - k_2 a\frac{\Omega_1^{i+k_1,j+k_2} + \Omega_1^{i,j}}{2} \tag{7}$$

$$\delta_1^{k_1,k_2} = \Omega_1^{i+k_1,j+k_2} - \Omega_1^{i,j} \tag{8}$$

$$\delta_2^{k_1,k_2} = \Omega_2^{i+k_1,j+k_2} - \Omega_2^{i,j} \tag{9}$$

$$\delta_3^{k_1,k_2} = \Omega_3^{i+k_1,j+k_2} - \Omega_3^{i,j} \tag{10}$$

Horizontal interfaces $(k_1, k_2 = \pm 1)$:

Let e^h be the thickness of the real horizontal joint; $S_h = \frac{b}{2}t$ the area of the horizontal interface, $I_{h1} = \frac{bt^3}{24}$ its inertia with respect to the y_1 axis and $I_{h3} = \frac{b^3t}{96}$ its inertia with respect to the y_3 axis. By denoting with $[[\mathbf{u}]]$ the jump of the displacement field at the Σ_{k_1,k_2} interface, the following expression of the horizontal interface elastic energy may be obtained:

$$\begin{aligned} W^{k_1,k_2} &= \frac{1}{2}\int_{\Sigma_{k_1,k_2}} [[\mathbf{u}]]\mathbf{K}[[\mathbf{u}]] \\ &= \frac{1K''}{2e^h}\left(S_h\left[(\Delta_1^{k_1,k_2})^2 + (\Delta_3^{k_1,k_2})^2\right] + (I_{h1}+I_{h3})(\delta_2^{k_1,k_2})^2\right) + \frac{1K'}{2e^h}\left(S_h(\Delta_2^{k_1,k_2})^2 + I_{h3}(\delta_3^{k_1,k_2})^2 + I_{h1}(\delta_1^{k_1,k_2})^2\right) \end{aligned} \tag{11}$$

where $K' = 2\mu^M + \lambda^M$ and $K'' = \mu^M$. The forces and the moments that the $B_{i+k_1,j+k_2}$ block applies to the $B_{i,j}$ block (Fig. 2) are:

$$-\frac{\partial W^{k_1,k_2}}{\partial u_1^{i,j}} = \frac{K''}{e^h}S_h\Delta_1^{k_1,k_2} \tag{12}$$

$$-\frac{\partial W^{k_1,k_2}}{\partial u_2^{i,j}} = \frac{K'}{e^h}S_h\Delta_2^{k_1,k_2} \tag{13}$$

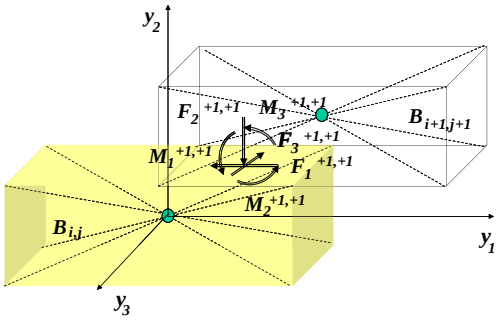

Fig. 2. Forces and moments at the horizontal interface.

$$-\frac{\partial W^{k_1,k_2}}{\partial u_3^{i,j}} = \frac{K''}{e^h} S_h \Delta_3^{k_1,k_2} \tag{14}$$

$$-\frac{\partial W^{k_1,k_2}}{\partial \Omega_1^{i,j}} = \frac{K'}{e^h} I_{h1} \delta_1^{k_1,k_2} + \frac{K''}{2e^h} S_h k_2 a \Delta_3^{k_1,k_2} \tag{15}$$

$$-\frac{\partial W^{k_1,k_2}}{\partial \Omega_2^{i,j}} = \frac{K''}{e^h} (I_{h1} + I_{h3}) \delta_2^{k_1,k_2} - \frac{K''}{4e^h} S_h k_1 b \Delta_3^{k_1,k_2} \tag{16}$$

$$-\frac{\partial W^{k_1,k_2}}{\partial \Omega_3^{i,j}} = \frac{K'}{e^h} I_{h3} \delta_3^{k_1,k_2} - \frac{K''}{2e^h} S_h k_2 a \Delta_1^{k_1,k_2} + \frac{K'}{4e^h} S_h k_1 b \Delta_2^{k_1,k_2} \tag{17}$$

Vertical interfaces $(k_1 = \pm 2, k_2 = 0)$:

Let e^v be the thickness of the real vertical joint; $S_v = at$ the area of the vertical interface, $I_{v2} = \frac{at^3}{12}$ its inertia with respect to the y_2 axis and $I_{v3} = \frac{a^3 t}{12}$ its inertia with respect to the y_3 axis. The following expression of the vertical interface elastic energy may be obtained:

$$\begin{aligned} W^{k_1,k_2} &= \frac{1}{2} \int_{\Sigma_{k_1,k_2}} [[\mathbf{u}]] \mathbf{K} [[\mathbf{u}]] \\ &= \frac{1K''}{2e^v} \left(S_v \left[(\Delta_2^{k_1,k_2})^2 + (\Delta_3^{k_1,k_2})^2 \right] + (I_{v2} + I_{v3}) (\delta_1^{k_1,k_2})^2 \right) + \frac{1K'}{2e^v} \left(S_v (\Delta_1^{k_1,k_2})^2 + I_{v3} (\delta_3^{k_1,k_2})^2 + I_{v2} (\delta_2^{k_1,k_2})^2 \right) \end{aligned} \tag{18}$$

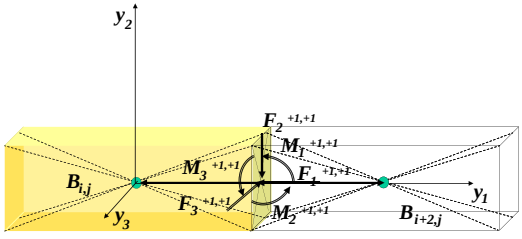

Fig. 3. Forces and moments at the vertical interface.

The forces and the moments that the $B_{i+k_1,j+k_2}$ block applies to the $B_{i,j}$ block (Fig. 3) are:

$$-\frac{\partial W^{k_1,k_2}}{\partial u_1^{i,j}} = \frac{K'}{e^v} S_v \Delta_1^{k_1,k_2} \tag{19}$$

$$-\frac{\partial W^{k_1,k_2}}{\partial u_2^{i,j}} = \frac{K''}{e^v} S_v \Delta_2^{k_1,k_2} \tag{20}$$

$$-\frac{\partial W^{k_1,k_2}}{\partial u_3^{i,j}} = \frac{K''}{e^v} S_v \Delta_3^{k_1,k_2} \tag{21}$$

$$-\frac{\partial W^{k_1,k_2}}{\partial \Omega_1^{i,j}} = \frac{K''}{e^v} (I_{v2} + I_{v3}) \delta_1^{k_1,k_2} \tag{22}$$

$$-\frac{\partial W^{k_1,k_2}}{\partial \Omega_2^{i,j}} = \frac{K'}{e^v} I_{v2} \delta_2^{k_1,k_2} - \frac{K''}{4e_v} S_v k_1 b \Delta_3^{k_1,k_2} \tag{23}$$

$$-\frac{\partial W^{k_1,k_2}}{\partial \Omega_3^{i,j}} = \frac{K'}{e^v} I_{v3} \delta_3^{k_1,k_2} + \frac{K''}{4e^v} S_v k_1 b \Delta_2^{k_1,k_2} \tag{24}$$

The following notations are introduced: $\mathbb{u}^{\mathrm{ip}}$ is the vector of in-plane degrees of freedom and $\mathbb{u}^{\mathrm{op}}$ is the vector of out of plane degrees of freedom.

$$\mathbb{u}^{\mathrm{ip}} = (u_1^{i,j}, u_2^{i,j}, \Omega_3^{i,j})^{\mathrm{T}}, \quad \mathbb{u}^{\mathrm{op}} = (u_3^{i,j}, \Omega_1^{i,j}, \Omega_2^{i,j})^{\mathrm{T}} \tag{25}$$

At present, one can easily check that the in plane elastic actions $\mathbb{F}^{\mathrm{ip}}_{\mathrm{elastic}}$ and the out of plane elastic actions $\mathbb{F}^{\mathrm{op}}_{\mathrm{elastic}}$ are uncoupled, hence the two problems may be studied separately:

$$\mathbb{F}^{\mathrm{ip}}_{\mathrm{elastic}} = -\frac{\partial W}{\partial \mathbb{u}^{\mathrm{ip}}} = -\mathbb{K}^{\mathrm{ip}} \mathbb{u}^{\mathrm{ip}} \tag{26}$$

$$\mathbb{F}^{\mathrm{op}}_{\mathrm{elastic}} = -\frac{\partial W}{\partial \mathbb{u}^{\mathrm{op}}} = -\mathbb{K}^{\mathrm{op}} \mathbb{u}^{\mathrm{op}} \tag{27}$$

and,

$$\mathbb{K}^{\mathrm{ip}} \mathbb{u}^{\mathrm{ip}} = \mathbb{F}^{\mathrm{ip}}_{\mathrm{ext}} \tag{28}$$

$$\mathbb{K}^{\mathrm{op}} \mathbb{u}^{\mathrm{op}} = \mathbb{F}^{\mathrm{op}}_{\mathrm{ext}} \tag{29}$$

Here W is the total elastic energy, $\mathbb{F}^{\mathrm{ip}}_{\mathrm{ext}}$ is the vector of the applied in plane actions, $\mathbb{F}^{\mathrm{op}}_{\mathrm{ext}}$ is the vector of the applied out of plane actions, $\mathbb{K}^{\mathrm{ip}}$ is the in plane stiffness matrix and $\mathbb{K}^{\mathrm{op}}$ is the out of plane stiffness matrix. Further details on the solution of Eqs. (28) and (29) are reported in Appendix A. The study below will be restricted to out of plane actions.

$$\mathbb{u}^{\mathrm{ip}} = 0, \quad \mathbb{F}^{\mathrm{ip}}_{\mathrm{ext}} = 0$$

3. The Reissner–Mindlin plate model

It is well-known that when the ratio of the thickness of a homogeneous plate over its overall size goes to zero, then the 3D solution converges to the Love–Kirchhoff solution. Caillerie (1984) has extended this

result to periodic plates. The method proposed below is an heuristic identification method which is not based on the standard homogenisation methods because these methods do not lead to a Reissner–Mindlin model. More precisely, on the basis of the theoretical homogenisation results of Caillerie (1984), it can be shown that the 3D discrete model can be accurately approximated by a Love–Kirchhoff homogeneous plate model, under the following three assumptions: (1) a, b and t are of the same order, (2) the considered structure is large enough and (3) the applied actions are smooth enough.

The elastic constants $D^F_{\alpha\beta\gamma\delta}$ which relate the plate bending tensor $(M_{\alpha\beta})$ to the curvature tensor $(\chi_{\alpha\beta}) = (-U^{LK}_{3,\alpha\beta})$:

$$M_{\alpha\beta} = D^F_{\alpha\beta\gamma\delta}\chi_{\gamma\delta} \quad \alpha,\beta,\gamma,\delta = 1,2 \tag{30}$$

have been identified by Cecchi and Sab (2002b) as follows:

$$D^F_{1111} = \frac{t^3}{12}\frac{4K'\frac{e^h}{a} + \frac{b}{a}K''\frac{e^v}{a}}{4\frac{e^h}{a}\frac{e^v}{b}} \tag{31}$$

$$D^F_{1122} = 0 \tag{32}$$

$$D^F_{2222} = \frac{t^3}{12}\frac{K'}{\frac{e^h}{a}} \tag{33}$$

$$D^F_{1212} = \frac{t}{192}\frac{K''\left(\frac{4e^h}{a}(a^2+t^2) + \frac{4e^v}{b}(b^2+t^2)\right) + K'\frac{b}{a}\frac{e^v}{a}t^2}{\frac{e^h}{a}\frac{e^v}{b}} \tag{34}$$

Starting from Eq. (1), the 3D displacement field in the discrete model is

$$\mathbf{u}(\mathbf{y}) = \begin{pmatrix} +\Omega^{i,j}_2 y_3 \\ -\Omega^{i,j}_1 y_3 \\ u^{i,j}_3 + \Omega^{i,j}_1(y_2 - y^{i,j}_2) - \Omega^{i,j}_2(y_1 - y^{i,j}_1) \end{pmatrix} \quad \forall \mathbf{y} \in B_{i,j} \tag{35}$$

In the Love–Kirchhoff model, the 3D displacement field is expressed in terms of displacement $U^{LK}_3(y_1,y_2)$ as follows:

$$\mathbf{u}^{LK}(\mathbf{y}) = \begin{pmatrix} -U^{LK}_{3,1}(y_1,y_2)y_3 \\ -U^{LK}_{3,2}(y_1,y_2)y_3 \\ U^{LK}_3(y_1,y_2) \end{pmatrix} \quad \forall \mathbf{y} \tag{36}$$

An identification between the Love–Kirchhoff model and the 3D discrete model may be performed as

$$u^{i,j}_3 = +U^{LK}_3(\mathbf{y}^{i,j}) \tag{37}$$

$$\Omega^{i,j}_2 = -U^{LK}_{3,1}(\mathbf{y}^{i,j}) \tag{38}$$

$$\Omega^{i,j}_1 = +U^{LK}_{3,2}(\mathbf{y}^{i,j}) \tag{39}$$

A Reissner–Mindlin orthotropic plate model is proposed so as to take into account shear effects. It must be noted that in this model, the 3D displacement field depends on displacement $U^{RM}_3(y_1,y_2)$ and two rotations $\phi_1(y_1,y_2)$ and $\phi_2(y_1,y_2)$ as follows:

$$\mathbf{u}^{RM}(\mathbf{y}) = \begin{pmatrix} \phi_1(y_1,y_2)y_3 \\ \phi_2(y_1,y_2)y_3 \\ U_3^{RM}(y_1,y_2) \end{pmatrix} \quad \forall \mathbf{y} \tag{40}$$

Similarly to the previous procedure, an identification between the Reissner–Mindlin model and the 3D discrete model may be defined as

$$u_3^{i,j} = +U_3^{RM}(\mathbf{y}^{i,j}) \tag{41}$$

$$\Omega_2^{i,j} = +\phi_1(\mathbf{y}^{i,j}) \tag{42}$$

$$\Omega_1^{i,j} = -\phi_2(\mathbf{y}^{i,j}) \tag{43}$$

In the Reissner–Mindlin model, the curvature tensor is $(\chi_{\alpha\beta}) = ((\phi_{\beta,\alpha} + \phi_{\alpha,\beta})/2)$. The bending elastic constants must be the same as those of the Love–Kirchhoff model (30)–(34) because these two models are asymptotically equivalent when the ratio t/L goes to zero. In a Reissner–Mindlin orthotropic plate model, the shear elastic constants $(F_{\alpha\beta})$ relate the shear stress vector (Q_α) to the shear strain vector $(U_{3,\alpha}^{RM} + \phi_\alpha)$ as follows:

$$Q_1 = F_{11}(U_{3,1}^{RM} + \phi_1), \quad Q_2 = F_{22}(U_{3,2}^{RM} + \phi_2), \quad F_{12} = 0. \tag{44}$$

The identification of F_{22} may be obtained from (14). Indeed, the Q_2 Reissner–Mindlin shear force component may be identified with the normalised resultant force in direction 3 exerted by blocks $B_{i+1,j+1}$ and $B_{i-1,j+1}$ on the horizontal interfaces $\Sigma_{+1,+1}$ and $\Sigma_{-1,+1}$ of block $B_{i,j}$:

$$\begin{aligned} Q_2 &= \frac{1}{b}\left(-\frac{\partial W^{+1,+1}}{\partial u_3^{i,j}} - \frac{\partial W^{-1,+1}}{\partial u_3^{i,j}} \right) \\ &= \frac{K''}{e^h}\frac{t}{2}\left(u_3^{i+1,j+1} - u_3^{i,j} + \frac{b}{2}\frac{\Omega_2^{i+1,j+1} + \Omega_2^{i,j}}{2} - a\frac{\Omega_1^{i+1,j+1} + \Omega_1^{i,j}}{2} \right) \\ &\quad + \frac{K''}{e^h}\frac{t}{2}\left(u_3^{i-1,j+1} - u_3^{i,j} - \frac{b}{2}\frac{\Omega_2^{i-1,j+1} + \Omega_2^{i,j}}{2} - a\frac{\Omega_1^{i-1,j+1} + \Omega_1^{i,j}}{2} \right) \end{aligned} \tag{45}$$

Introducing (41)–(43) in (45) with Taylor expansions of order 1 in U_3^{RM} and of order 0 in ϕ_1 and ϕ_2, (45) becomes:

$$Q_2 = \frac{K''at}{e^h}(U_{3,2}^{RM} + \phi_2) \tag{46}$$

Therefore, the elastic shear constant $F_{22} = \frac{K''at}{e^h}$ has been identified.

Similarly, the Reissner–Mindlin shear constant F_{11} may be found with (21). The $B_{i,j}$ block is in contact with the $B_{i+2,j}$ block through the interface $\Sigma_{+2,0}$. Hence the normalised shear force that $B_{i+2,j}$ applies to $B_{i,j}$ is

$$Q_1 = -\frac{1}{a}\frac{\partial W^{+2,0}}{\partial u_3^{i,j}} = \frac{K''t}{e^v}\left(u_3^{i+2,j} - u_3^{i,j} + b\frac{\Omega_2^{i+2,j} + \Omega_2^{i,j}}{2} \right) \tag{47}$$

Introducing (41)–(43) in (47) with Taylor expansions of order 1 in U_3^{RM} and of order 0 in ϕ_1 and ϕ_2, (47) becomes:

$$Q_1 = \frac{K''bt}{e^v}(U_{3,1}^{RM} + \phi_1) \tag{48}$$

Therefore, the elastic shear constant $F_{11} = \frac{K''bt}{e^v}$ has been identified.

Remark. The 3D stress vector in the mortar can be computed in terms of the Reissner–Mindlin displacement and rotations by using (2) and (41)–(43). In particular, if the mortar joints are modelled as Coulomb interfaces, the limit of the assumption of purely elastic mortar can be established.

4. Numerical results: a comparison between the three models

In this section, a comparison between Love–Kirchhoff model, Reissner–Mindlin model and the 3D discrete model is conducted on a test case. As explained in Section 2, in plane and out of plane actions are uncoupled and only the case of out of plane actions is here studied.

A plate, simply supported on four edges, is subject to an uniform force distribution, p, in the orthogonal direction to the middle plane (Fig. 4). For the 3D discrete model, this loading corresponds to an external force, abp, applied in direction 3 to each brick's center inside the plate, and to condition $u_3^{i,j} = 0$ applied to each brick's center of the boundary. The plate dimensions are: L, H and t (thickness). The balance equations for plate models are:

$$M_{\alpha\beta,\beta} - Q_\alpha = 0 \tag{49}$$

$$Q_{\alpha,\alpha} - p = 0 \tag{50}$$

The bending constitutive law is (30)–(34) with $(\chi_{\alpha\beta}) = (-U^{LK}_{3,\alpha\beta})$ for the Love–Kirchhoff model and $(\chi_{\alpha\beta}) = ((\phi_{\beta,\alpha} + \phi_{\alpha,\beta})/2)$ for the Reissner–Mindlin model. The shear constitutive law is (46) and (48) for the Reissner–Mindlin model.

The details of the analytical procedure to solve the problem are reported in Appendix B. The Navier double series expansion and suitable boundary conditions are used to calculate the coefficients S_{mn} that characterise the solution of the form:

$$U_3(x_1, x_2) = \sum_{m=1}^{\infty} \sum_{n=1}^{\infty} S_{mn} \sin\frac{m\pi x_1}{L} \sin\frac{n\pi x_2}{H} \tag{51}$$

It is clear that, when the number of heterogeneity is large enough, the homogenised plate models should be consistent with the discrete 3D numerical model. More precisely, according to Caillerie (1984), the Love–Kirchhoff model is consistent when block thickness and block in plane dimension are of the same order; all these dimensions being small by comparison with the overall plate dimension. So three numerical experimentations are carried out. The thickness being fixed, the first experimentation is performed aiming at

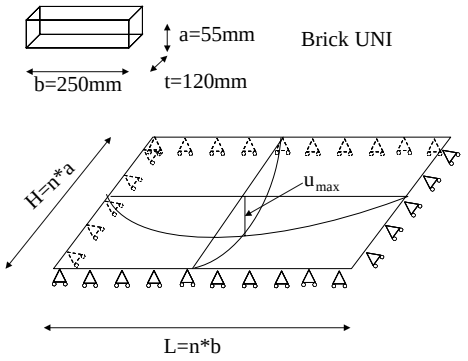

Fig. 4. Plate dimensions and boundary conditions.

identifying the minimum number of blocks for which the hypothesis of masonry modelled as a homogeneous Love–Kirchhoff plate may be used. The second experimentation is performed so as to identify the minimum number of blocks for which the hypothesis of masonry modelled as a homogeneous Reissner–Mindlin plate may be used. The number of blocks being fixed, the third experimentation is performed so as to identify the critical panel thickness for which the hypothesis of Love–Kirchhoff plate and Reissner–Mindlin plate are acceptable.

4.1. Experimentation n.1

The case of a rectangular simply supported plate subject to a uniform distributed load orthogonal to the middle surface of the plate has been proposed. A comparison between the displacement field obtained from the homogenised Love–Kirchhoff plate model and the discrete numerical model has been carried out. The analysed plate is composed of n blocks both in horizontal and vertical direction (Fig. 4). The blocks are modelled as rigid bodies connected by elastic interfaces. The block dimensions are 250 mm (width), 55 mm (height) and 120 mm (or 180 mm) (thickness). In this case the hypothesis $\zeta \approx \varepsilon$ is relevant. The mortar joint thickness is 2 mm, the Young modulus is $E^M = 1000$ MPa and Poisson ratio is $\nu^M = 0.2$.

In Fig. 4 the qualitative deformation of the middle line in horizontal direction is presented. The maximum error between the two models is referred to the maximum displacement $u_{\max}$ in the centre of the plate. The deformed configuration has been normalised with respect to the analytical value of $u_{\max}$. In Fig. 5, the $e_{\%}$ percent error in $u_{\max}$ has been presented as a function of n. The $e_{\%}$ is defined as follows:

$$e_{\%} = 100 \frac{u_{\max}^{\text{numerical}} - u_{\max}^{\text{analytical}}}{u_{\max}^{\text{analytical}}}$$

Fig. 5 clearly shows that the error quickly decreases when the number of blocks in the panel increases. It is clear that the error is negligible when the number of blocks in the panel is greater than $n = 21$. This

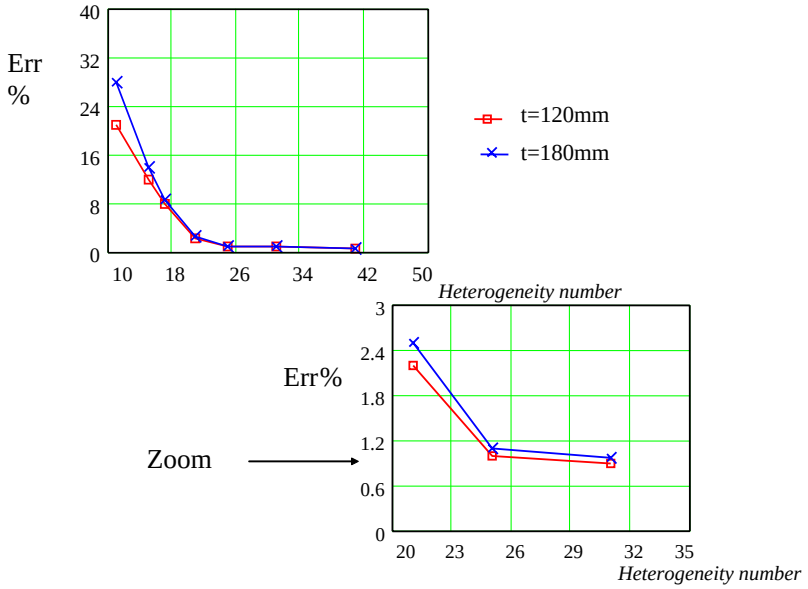

Fig. 5. Percentual error versus heterogeneity number between Love–Kirchhoff plate model and 3D discrete model.

heterogeneity number can be assumed as a critical value to use the homogenised Love–Kirchhoff model. In particular two trends of $e_{\%}$ percent error are reported for two values of block thickness: 120 and 180 mm.

Moreover, it is interesting to note that the Love–Kirchhoff model is stiffer than the 3D discrete one. This aspect is connected to the plate model hypothesis: middle surface of the plate indeformable and transverse shear deformation neglected. Hence the $e_{\%}$ percent error has a positive value.

4.2. Experimentation n.2

The same experimentation has been carried out when the continuum model to compare the 3D discrete one is a homogenised Reissner–Mindlin plate. Hence, also in this experimentation, the parameter that varies is the n number of blocks both in horizontal and vertical direction. In Fig. 6 the two cases of plate thickness 120 and 180 mm are reported.

It is interesting to note the Mindlin–Reissner model is more consistent than the Love–Kirchhoff one also in the case of number of blocks less than $n = 21$. This aspect can be connected to the ratio between the L overall dimension of the plate and the t thickness of the plate according to the plate theory. In fact when the number of blocks in the plate is not relevant, the 2D reference model cannot be a thin plate model—Love–Kirchhoff plate—, the thickness dimension is not small enough if compared to the overall in plane plate dimension. Hence a thick plate model—Mindlinn-Reissner plate—is more consistent.

Moreover, in this second experimentation it is interesting to note that the Reissner–Mindlin model is more deformable than the 3D discrete model. This aspect is connected to the shear elastic constants,—see Section 3—, which have been imposed in addition to the flexural homogenised constants. Hence the $e_{\%}$ percent error has a negative value.

4.3. Experimentation n.3

For the same plate with fixed n—$n = 21$ and $n = 25$—, the two homogenised models are compared when the t thickness of the block—that is also the thickness of the plate as a whole—varies from 120 to 600 mm.

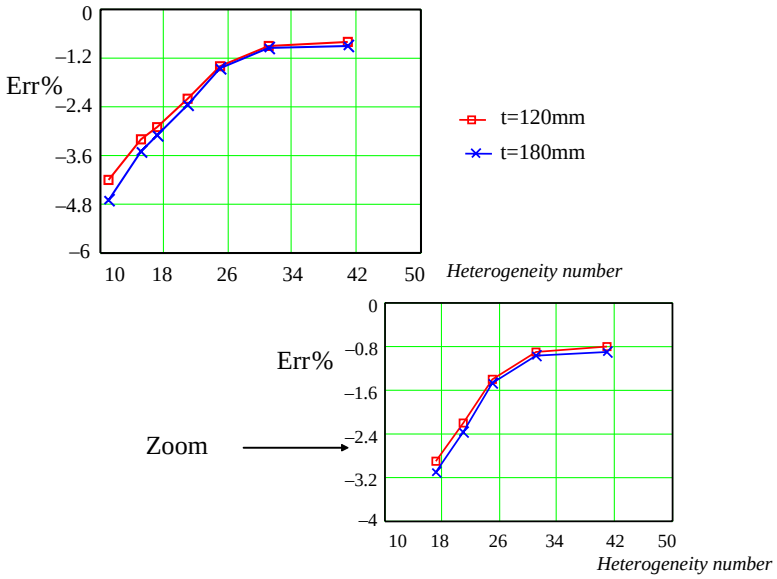

Fig. 6. Percentual error versus heterogeneity number between Reissner–Mindlin plate model and 3D discrete model.

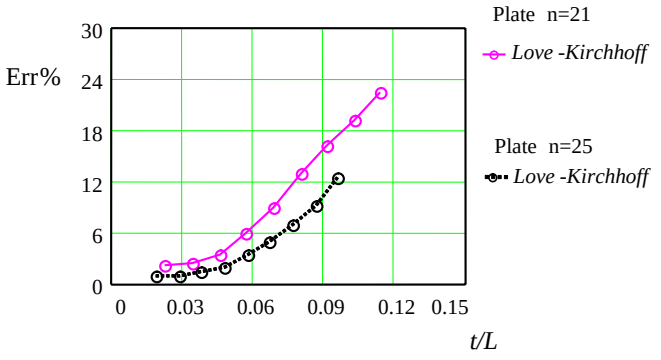

Fig. 7. Percentual error versus the ratio between the thickness and the L dimension of plate-under Love–Kirchhoff hypothesis.

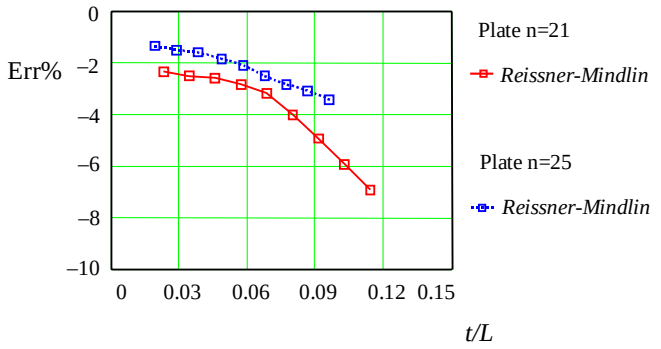

Fig. 8. Percentual error versus the ratio between the thickness and the L dimension of plate-under Reissner–Mindlin hypothesis.

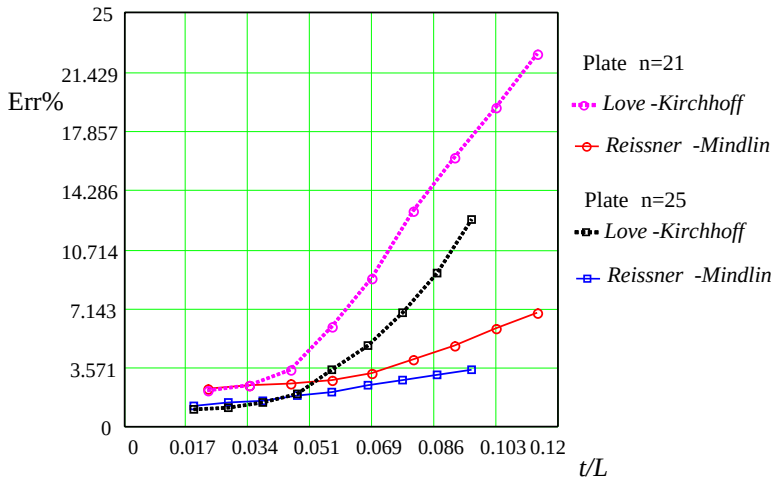

Fig. 9. Absolute percentual error versus the ratio between the thickness and the L dimension of plate-under Love–Kirchhoff and Reissner–Mindlin hypothesis.

Hence, the ratio between the t thickness and the L dimension of the plate (see Fig. 4) varies from 0.023 to 0.114 for the plate with $n = 21$, and from 0.019 to 0.096 for the plate with $n = 25$. The normalisation has been realised versus the L dimension of the plate. The ratio between the two dimensions of the plate $\frac{L}{H}$ is 4.54.

Starting from the thin plate Love–Kirchhoff hypothesis it is clear that the error significantly increases when the thickness of the plate increases. In Fig. 7, for $n = 21$ and $n = 25$ the $e_{\%}$ percent error is plotted. Clearly there appears that the identification between a 3D body and a 2D body under the Love–Kirchhoff hypothesis is very sensitive to the thickness of the plate, so the shear deformation cannot be neglected. A comparison between the 3D discrete model and the Reissner–Mindlin plate model is carried out. Fig. 8 clearly shows that the Reissner–Mindlin model is very consistent also for the high thickness of the plate. Fig. 9 shows a global comparison for the two plate models. For the sake of simplicity in this figure the absolute values of the $e_{\%}$ percent error is used.

5. Conclusions

In this work a comparison between a 3D numerical discrete model and two homogenised plate models has been performed. The idea was both to verify the limit of application of the homogenised models and to set the parameters present in these models by comparison with the discrete model. The perspective of development of the discrete model is a study both in a non-linear field—i.e. mortar modelled as no tension material—and in a dynamic field.

The more consistent contribution of this work is in the formulation of the Reissner–Mindlin model. The bending constants are the same as those of the Love–Kirchhoff model, hence obtained from a homogenisation field problem. On the other hand, the shear constants has been obtained through an identification on the shear forces in the discrete model and the Reissner–Mindlin one. As shown in the three numerical experimentations, by comparison with the Love–Kirchhoff model, the Reissner–Mindlin plate model fits in a more consistent manner the results of the discrete model.

Appendix A. Numerical procedure

Although standard methods exist to solve numerically (28) and (29), a Molecular Dynamics method (Allen and Tildesley, 1994; Owen and Hinton, 1980) has been developped in the perspective of linear and non-linear analysis with dynamic loading. In this case, the equation to be solved is

$$\mathbb{u} = (u_k^{i,j}, \Omega_k^{i,j})^{\mathrm{T}}, \quad k = 1,3 \tag{A.1}$$

$$\mathbb{M}\frac{\partial^2 \mathbb{u}}{\partial t^2} + \mathbb{K}\left(\mathbb{u} + \mu\frac{\partial \mathbb{u}}{\partial t}\right) = \mathbb{F}_{\mathrm{ext}} \tag{A.2}$$

where μ is a damping coefficient, $\mathbb{F}_{\mathrm{ext}}$ are the applied actions, $\mathbb{M}$ is the (diagonal) mass matrix and $\mathbb{K}$ the stiffness matrix.

To solve the dynamic Eq. (A.2) the predictor–corrector algorithm GEAR of order 2 is used. Let $\mathbb{u}(t)$, $\mathbb{v}(t)$ and $\mathbb{a}(t)$ denote the displacement, the velocity and the acceleration at time t. Using a Taylor expansion the correspondent predictor vectors at time $t + \delta t$ are:

$$\mathbb{u}^p(t+\delta t) = \mathbb{u}(t) + \delta t \cdot \mathbb{v}(t) + \frac{1}{2}\delta t^2 \cdot \mathbb{a}(t) + \mathrm{o}(\delta t^3) \tag{A.3}$$

$$\mathbb{v}^p(t+\delta t) = \mathbb{v}(t) + \delta t \cdot \mathbb{a}(t) + \mathrm{o}(\delta t^2) \tag{A.4}$$

$$\mathbb{a}^p(t+\delta t) = \mathbb{a}(t) + \mathrm{o}(\delta t) \tag{A.5}$$

Using the balance equation, the real accelerations may be found:

$$\mathbb{a} = \mathbb{M}^{-1}(\mathbb{F}_{\text{ext}} - \mathbb{K}(\mathbb{u}^p + \mu \mathbb{v}^p)) \tag{A.6}$$

and the error in the predictor time step may be calculated:

$$\delta\mathbb{a}(t+\delta t) = \mathbb{a} - \mathbb{a}^p(t+\delta t) \tag{A.7}$$

Finally, the corrector time step is introduced:

$$\mathbb{u}(t+\delta t) = \mathbb{u}^p(t+\delta t) + \frac{1}{4}\delta t^2 \cdot \delta\mathbb{a} \cdot c_0 \tag{A.8}$$

$$\mathbb{v}(t+\delta t) = \mathbb{v}^p(t+\delta t) + \frac{1}{2}\delta t \cdot \delta\mathbb{a} \cdot c_1 \tag{A.9}$$

$$\mathbb{a}(t+\delta t) = \mathbb{a}^p(t+\delta t) + \delta\mathbb{a} \cdot c_2 \tag{A.10}$$

where $c_0 = 0$, $c_1 = 1$ and $c_2 = 1$. In the special case of static equilibrium (Fig. 10) the time step integration is stopped when:

$$e_{\text{num}} = \|\mathbb{K}\mathbf{u}^p - \mathbf{F}_{\text{ext}}\| < \text{toler} \tag{A.11}$$

In the above formula, the force balance equations are normalised by a typical applied force (for instance, pab in the case considered in Section 4) and the moment balance equations are normalised by a typical applied moment (for instance, pab^2 in the case considered in Section 4). In this case, the used norm is the maximum absolute value and the tolerance is 0.005. In other words, the maximum error in the force balance equations is less than $0.005pab$ and the maximum error in the moment balance equations is less than $0.005pab^2$.

The δt time step must be much smaller than a critical value T_c calculated as a function of mass and stiffness properties of the block. So

$$\delta t = \frac{T_c}{100} \quad T_c = \sqrt{\frac{m}{k_n}} \quad k_n = \frac{S_h K'}{e^v} \quad m = \rho abt \quad \mu = \sqrt{m \cdot k_n} \tag{A.12}$$

where ρ is the density of the block.

The developed software is written in Fortran. The program formulation starts from geometrical description of a generic masonry wall. Each block is identified with its centre position. As shown in Fig. 11 a wall with k-block courses has been investigated: odd courses present n-blocks, while even courses present n+1 blocks—hence the length between both two even courses and two odd courses is $2n + 1$—. Moreover in the even courses the first and the last blocks are half-blocks. This is due to the running bond texture of masonry.

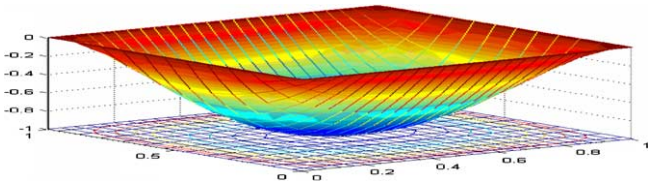

Fig. 10. Final equilibrated configuration.

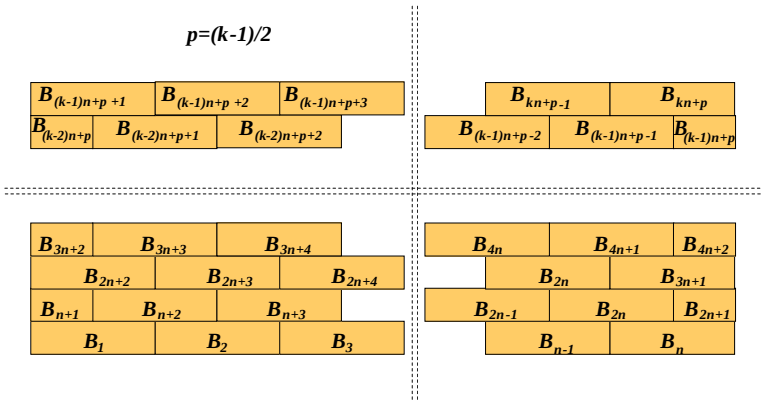

Fig. 11. Geometrical description of a generic masonry wall.

The following steps are proposed:

- definition of geometrical and mechanical quantities;
- construction of mass tensor for the generic i-block;
- imposition of the boundary condition on forces—applied loads—and on displacement—constraint degrees of freedom—;
- step 0: the initial displacements, velocities and accelerations are set to zero;
- step i: computation of the predicted displacements, velocities and accelerations (A.3)–(A.5);
- evaluation of elastic and damping forces and moments at the interfaces according to Section 2 procedure;
- if the static equilibrium according to Eq. (A.11) is satisfied, then stop;
- evaluation of real acceleration at the i-step according to Eq. (A.6);
- evaluation of the corrected displacements, velocities and accelerations (A.8)–(A.10);
- go to step $i+1$.

In this analysis, when the plate is about to the configuration of static equilibrium, the kinetic energy may be still consistent. The plate fluctuates around this configuration. In order to quicken the convergence, the evaluation of the kinetic energy has been performed at each step. If at the $i+1$ time step the kinetic energy is smaller than the kinetic energy at the i step, then the velocity vector is set to zero.

Appendix B. Analytical formulation of simply supported orthotropic plate

1. Love–Kirchhoff plate

The equations to be solved are (30) and (49) and (50) with $(\chi_{\alpha\beta}) = (-U_{3,\alpha\beta})$. Therefore, the differential equation of the plate is

$$D^F_{1111}U_{3,1111} + 2(D^F_{1122} + 2D^F_{1212})U_{3,1122} + D^F_{2222}U_{3,2222} = p(x_1, x_2) \tag{B.1}$$

The boundary conditions of a simply supported plate on the four edges are:

$$\begin{cases} U_3 = 0; & U_{3,11} + \nu_{21}U_{3,22} = 0 \quad \text{for } x_1 = 0;\ x_1 = L \\ U_3 = 0; & U_{3,22} + \nu_{12}U_{3,11} = 0 \quad \text{for } x_2 = 0;\ x_2 = H \end{cases} \tag{B.2}$$

where $v_{21} = \frac{D^F_{1122}}{D^F_{1111}} = 0$ and $v_{12} = \frac{D^F_{1122}}{D^F_{2222}} = 0$. The boundary conditions will be satisfied by any of the terms of

$$U_3(x_1, x_2) = \sum_{m=1}^{\infty} \sum_{n=1}^{\infty} S_{mn} \sin\frac{m\pi x_1}{L} \sin\frac{n\pi x_2}{H} \tag{B.3}$$

where S_{mn} are unknown coefficients, m and n are integers. The load is as follows:

$$p(x_1, x_2) = \sum_{m=1}^{\infty} \sum_{n=1}^{\infty} p_{mn} \sin\frac{m\pi x_1}{L} \sin\frac{n\pi x_2}{H} \tag{B.4}$$

so, the p_{mn} coefficients are:

$$p_{mn} = \frac{4}{LH} \int_0^L \int_0^H p(x_1, x_2) \sin\frac{m\pi x_1}{L} \sin\frac{n\pi x_2}{H} \, dx_1 \, dx_2 \tag{B.5}$$

and by substituting (B.3) in the differential Eq. (B.1),

$$S_{mn} = \frac{p_{mn}}{D\pi^4} \tag{B.6}$$

with

$$D = D^F_{1111}\left(\frac{m}{L}\right)^4 + 2(D^F_{1122} + 2D^F_{1212})\left(\frac{mn}{HL}\right)^2 + D^F_{2222}\left(\frac{n}{H}\right)^4 \tag{B.7}$$

If the load is uniform $p(x_1, x_2) = p$, then

$$p_{mn} = \frac{4p}{mn\pi^2}(1 - \cos m\pi)(1 - \cos n\pi) \tag{B.8}$$

2. Reissner–Mindlin plate

The equations to be solved are (30), (46) and (48)–(50) with $(\chi_{\alpha\beta}) = ((\phi_{\beta,\alpha} + \phi_{\alpha,\beta})/2)$ for the Reissner–Mindlin model. Substituting the Eqs. (30), (46), (48) in (49), (50), one obtains

$$D^F_{1111}\phi_{1,11} + D^F_{1212}\phi_{1,22} + (D^F_{1122} + D^F_{1212})\phi_{2,12} - F_{11}(\phi_1 + U_{3,1}) = 0 \tag{B.9}$$

$$(D^F_{1122} + D^F_{1212})\phi_{1,12} + D^F_{1212}\phi_{2,11} + D^F_{2222}\phi_{2,22} - F_{22}(\phi_2 + U_{3,2}) = 0 \tag{B.10}$$

$$F_{11}(\phi_{1,1} + U_{3,11}) + F_{22}(\phi_{2,2} + U_{3,22}) - p(x_1, x_2) = 0 \tag{B.11}$$

In the case of simply supported plate, the boundary conditions are:

$$\begin{cases} U_3 = 0; \quad \phi_2 = 0; \quad \phi_{1,1} = 0 \quad \text{for } x_1 = 0;\ x_1 = L \\ U_3 = 0; \quad \phi_1 = 0; \quad \phi_{2,2} = 0 \quad \text{for } x_2 = 0;\ x_2 = H \end{cases} \tag{B.12}$$

The functions that satisfy the balance equation and the boundary conditions are (Dobyns, 1981):

$$U_3(x_1, x_2) = \sum_{m=1}^{\infty} \sum_{n=1}^{\infty} S_{mn} \sin\frac{m\pi x_1}{L} \sin\frac{n\pi x_2}{H} \tag{B.13}$$

$$\phi_1(x_1, x_2) = \sum_{m=1}^{\infty} \sum_{n=1}^{\infty} A_{mn} \cos\frac{m\pi x_1}{L} \sin\frac{n\pi x_2}{H} \tag{B.14}$$

$$\phi_2(x_1, x_2) = \sum_{m=1}^{\infty} \sum_{n=1}^{\infty} B_{mn} \sin\frac{m\pi x_1}{L} \cos\frac{n\pi x_2}{H} \tag{B.15}$$

$$p(x_1,x_2)=\sum_{m=1}^{\infty}\sum_{n=1}^{\infty}p_{mn}\sin\frac{m\pi x_1}{L}\sin\frac{n\pi x_2}{H} \tag{B.16}$$

Substituting these functions in the differential equations:

$$\begin{pmatrix} g_{11} & g_{12} & g_{13}\\ g_{12} & g_{22} & g_{23}\\ g_{13} & g_{23} & g_{33}\end{pmatrix}\begin{pmatrix} A_{mn}\\ B_{mn}\\ S_{mn}\end{pmatrix}=\begin{pmatrix} 0\\ 0\\ p_{mn}\end{pmatrix} \tag{B.17}$$

where

$$g_{11}=D^F_{1111}\left(\frac{m\pi}{L}\right)^2+D^F_{1212}\left(\frac{n\pi}{H}\right)^2+F_{11}$$

$$g_{12}=(D^F_{1122}+D^F_{1212})\frac{m\pi}{L}\frac{n\pi}{H}$$

$$g_{13}=F_{11}\frac{m\pi}{L}$$

$$g_{22}=D^F_{1212}\left(\frac{m\pi}{L}\right)^2+D^F_{2222}\left(\frac{n\pi}{H}\right)^2+F_{22}$$

$$g_{23}=F_{22}\frac{n\pi}{H}$$

$$g_{33}=F_{11}\left(\frac{m\pi}{L}\right)^2+F_{22}\left(\frac{n\pi}{H}\right)^2$$

solving the system, one obtains

$$A_{mn}=\frac{(g_{12}g_{23}-g_{22}g_{13})p_{mn}}{\det(g_{ij})} \tag{B.18}$$

$$B_{mn}=\frac{(g_{12}g_{13}-g_{11}g_{23})p_{mn}}{\det(g_{ij})} \tag{B.19}$$

$$S_{mn}=\frac{(g_{11}g_{22}-g_{12}^2)p_{mn}}{\det(g_{ij})} \tag{B.20}$$

where $\det(g_{ij})$ is the determinant of g_{ij}. Hence it is possible to evaluate the $u_3(x_1,x_2)$ displacement field and the $\phi_\alpha(x_1,x_2)$ rotations in the plate.

References

Alpa, G., Monetto, I., 1994. Microstructural model for dry block masonry walls with in-plane loading. J. Mech. Phys. Solids 47 (7), 1159–1175.

Allen, M.P., Tildesley, D.J., 1994. Computer Simulations of Liquids. Oxford Science Publications.

Anthoine, A., 1995. Derivation of in plane elastic characteristic of masonry through homogenization theory. Int. J. Solid Struct. 32, 137–163.

Anthoine, A., Pegon, P., 1994. Numerical strategies for solving continuum damage problems involving softening: application to the homogenization of masonry. In: Proceedings of the Second International Conference on Computational Structures Technology, Atene.

Avila-Pozos, O., Klarbring, A., Movchan, A.B., 1999. Asymptotic model of orthotropic highly inhomogeneous layered structure. Mech. Mater. 31, 101–115.

Caillerie, D., 1984. Thin elastic and periodic plates. Math. Meth. Appl. Sci. 6, 159–191.

Cecchi, A., Rizzi, N.L., 2001. Heterogeneous material. A mixed homogenization rigidification technique. Int. J. Solids Struct. 38 (1), 29–36.

Cecchi, A., Sab, K., 2002a. A multi-parameter homogenization study for modelling elastic masonry. Eur. J. Mech. A.-Solids 21, 249–268.

Cecchi, A., Sab, K., 2002b. Out of plane model for heterogeneous periodic materials: the case of masonry. Eur. J. Mech. A.-Solids 21, 715–746.

de Felice, G., 1995. Détermination des coefficients d'élasticité de la maçonnerie par une méthode d'homogénéisation. Actes du 12ème Congrès Français de Mécanique, vol. 1, Strasbourg, pp. 393–396.

Dobyns, A.L., 1981. The analysis of simply supported orthotropic plates subject to static and dynamic loads. Am. Inst. Aeronaut. Astronaut. J. (May), 642–650.

Klarbring, A., 1991. Derivation of model of adhesively bounded joints by the asymptotic expansion method. Int. J. Eng. Sci. 29, 493–512.

Lee, S.J., Pande, G.N., Middleton, J., Kralj, B., 1996. Numerical modelling of brick masonry panels subject to lateral loading. Comput. Struct. 31 (211), 473–479.

Lee, S.J., Pande, G.N., Kralj, B., 1998. A Comparative Study on the Approximate Analysis of Masonry Structures. Mater. Struct. 61 (4), 735–745.

Lofti, H.R., Benson Shing, P., 1994. Interface model applied to fracture of masonry structures. J. Struct. Eng. ASCE 120, 63–80.

Lopez, J., Oller, S., Onate, E., Lubliner, J., 1999. A homogeneous constitutive model for masonry. Int. J. Numer. Meth. Eng. 46, 1651–1671.

Lourenço, P.B., Rots, J. G., 1993. Discrete models for jointed block masonry walls. In: Proceedings of the Sixth North American Masonry Conference, Philadelphia, pp. 939–949.

Luciano, R., Sacco, E., 1997. Homogenization technique and damage model for old masonry material. Int. J. Solids Struct. 34 (24), 3191–3208.

Markov, K.Z., 1999. Elementary micromechanics of heterogeneous solids. In: Markov, K.Z., Preziosi, L. (Eds.), Heterogeneous Media Micromechanics Modeling Methods and Simulations. Birkhauser, Boston, pp. 1–162.

Masiani, R., Rizzi, N.L., Trovalusci, P., 1995. Masonry walls as structured continua. Meccanica 30, 673–683.

Owen, D.R.J., Hinton, E., 1980. Finite Elements in Plasticity: Theory and Practice. Pineridge Press Limited, Swansea U.K.

Salerno, G., de Felice G.,1999. Continuum modelling of periodic brickwork. Report no. 206 LABMEC. Dip. di Strutture, Univ. Calabria.

Salerno, G., de Felice, G., 2000. Continuum modelling of discrete systems: a variational approach. In: Proceedings of the ECCOMAS, Barcelona, pp. 11–14.

Sanchez-Palencia, E., 1980. Non Homogeneous Media and Vibration Theory. Springer, Berlin.

Sanchez-Palencia, E., Zaoui, A. (Eds.), 1987. Homogenization Techniques for Composite Media, Lectures Notes, vol. 272. Springer, Berlin.

Sanchez-Hubert, J., Sanchez-Palencia, E., 1992. Introduction aux méthodes asymptotiques et a l'homogénéisation. Masson, Paris.